nature neuroscience

Lack of cadherins Celsr2 and Celsr3 impairs ependymal ciliogenesis, leading to fatal hydrocephalus

Fadel Tissir[1,8], Yibo Qu[1,8], Mireille Montcouquiol[2], Libing Zhou[1], Kouji Komatsu[3,4], Dongbo Shi[4,5], Toshihiko Fujimori[3,4], Jason Labeau[1], Donatienne Tyteca[6], Pierre Courtoy[6], Yves Poumay[7], Tadashi Uemura[4,5] & Andre M Goffinet[1]

Ependymal cells form the epithelial lining of cerebral ventricles. Their apical surface is covered by cilia that beat in a coordinated fashion to facilitate circulation of the cerebrospinal fluid (CSF). The genetic factors that govern the development and function of ependymal cilia remain poorly understood. We found that the planar cell polarity cadherins Celsr2 and Celsr3 control these processes. In *Celsr2*-deficient mice, the development and planar organization of ependymal cilia are compromised, leading to defective CSF dynamics and hydrocephalus. In *Celsr2* and *Celsr3* double mutant ependyma, ciliogenesis is markedly impaired, resulting in lethal hydrocephalus. The membrane distribution of Vangl2 and Fzd3, two key planar cell polarity proteins, was disturbed in *Celsr2* mutants, and even more so in *Celsr2* and *Celsr3* double mutants. Our findings suggest that planar cell polarity signaling is involved in ependymal cilia development and in the pathophysiology of hydrocephalus, with possible implications in other ciliopathies.

© 2010 Nature America, Inc. All rights reserved.

Cilia are organelles that protrude from the apical surface of most eukaryotic cells. They are classified into three groups according to their structure and motility[1]. Primary monocilia, which are present in most cells, lack a central pair of microtubules (9+0 structure), and have several roles in mechanosensation and cell signaling. Nodal cilia have a 9+0 structure but, unlike primary cilia, they move and generate an asymmetric distribution of morphogenetic cues in the node, thereby contributing to laterality[2]. The third group comprises motile 9+2 cilia that cover the epithelial cells that line airways, reproductive tracts and cerebral ventricles. Motile cilia are crucial for clearing mucus and debris in the airways and might assist the transit of sperm and eggs in genital tracts[3,4]. In the early postnatal mammalian brain, neuroepithelial cells that line the cerebral ventricles leave the cell cycle and differentiate into a monolayer of ependymal cells. At the end of maturation, the apical surface of ependymal cells bears dozens of cilia that beat in coordinated manner to facilitate the circulation of the CSF, from sites of production in choroid plexuses to sites of absorption in subarachnoid spaces. In mice, mutations in genes involved in the assembly or structure of ependymal cilia, such as *Mdnah5* (ref. 5), *Ift88* (also known as *Tg737* or *Polaris*)[6] and *Hy3* (refs. 7,8) affect ciliogenesis, alter CSF dynamics and result in hydrocephalus. However, little is known about the genetic factors that govern the polarization of ependymal cilia and the relationship between polarity and the development and function of these organelles.

Planar cell polarity (PCP), also known as tissue polarity, controls the polarization of epithelial cells in a plane perpendicular to their apicobasal axis. It was initially described in *Drosophila*, where it affects the stereotypic arrangement of cuticular hairs, sensory bristles and ommatidia through the control of so-called 'core PCP genes' that include *Van Gogh*, *Frizzled*, *Flamingo* (also known as *Starry Night*), *Disheveled*, *Diego* and *Prickle*[9,10]. In mammals, PCP designates processes that control the development of polarized cellular structures and involve at least one core PCP gene ortholog[11]. PCP-dependent events include neural tube closure[12,13], hair bundle orientation in inner ear cells[13,14] and hair follicle patterning in the skin[15–17]. PCP-like mechanisms have also been implicated in dendrite morphogenesis[18] and axon guidance[19,20]. In the ciliated epidermis of larval *Xenopus*, morpholino downregulation experiments showed that *Disheveled1–3*, *Inturned* and *Fuzzy* are implicated in the control of the actin cytoskeleton and apical docking of ciliary basal bodies and that the planar orientation of multiciliate cells is disrupted when Disheveled, Vangl2 and Fuzzy signaling are altered[21,22], indicating that PCP signaling and ciliogenesis are linked.

In this work, we studied mice in which *Celsr2* and *Celsr3*, the murine orthologs of the *Drosophila* core PCP gene *Flamingo*, had been inactivated and show that deficiency of these two seven-pass transmembrane cadherins markedly disrupts the genesis of ependymal cilia, as well as the cellular partition of the PCP proteins Vangl2 and Fzd3, leading to lethal hydrocephalus.

RESULTS

Celsr2 mutant mice develop progressive hydrocephalus

We have previously described conditional and constitutive *Celsr3* mutant mice[23]. We generated the mutant *Celsr2* allele by inserting a

[1]Université catholique de Louvain, Institute of Neuroscience, Developmental Neurobiology, Brussels, Belgium. [2]INSERM, U862, Neurocentre Magendie, Molecular Basis of Planar Polarity Group, Bordeaux, France. [3]Division of Embryology, National Institute for Basic Biology, Okazaki Aichi, Japan. [4]CREST, Japan Science and Technology Agency, Tokyo, Japan. [5]Graduate School of Biostudies, Kyoto University, Kyoto, Japan. [6]Université catholique de Louvain, de Duve Institute, Brussels, Belgium. [7]Facultés universitaires Notre-Dame de la Paix, Namur, Belgium. [8]These authors contributed equally to this work. Correspondence should be addressed to F.T. (fadel.tissir@uclouvain.be) or A.M.G. (andre.goffinet@uclouvain.be).

Received 7 January; accepted 1 April; published online 16 May 2010; corrected online 23 May 2010 (details online); doi:10.1038/nn.2555

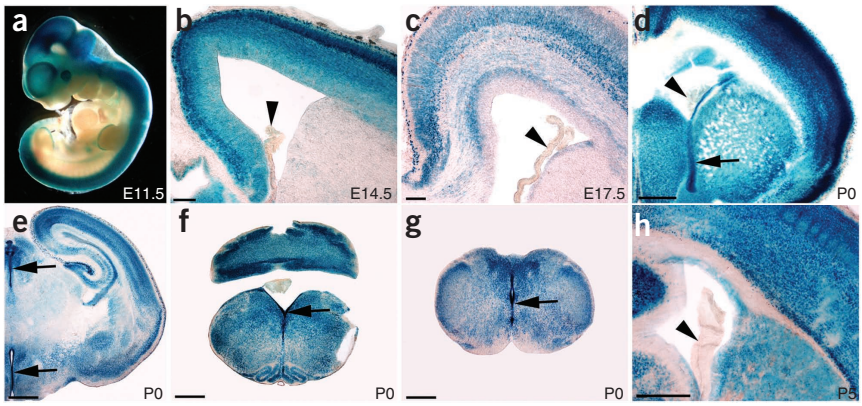

Figure 1 *Celsr2* is expressed in differentiating ependymal cells but not in choroid plexus. (**a**–**h**) Expression of *Celsr2* depicted by beta-galactosidase histochemistry in E11.5 embryo (**a**), and in brain coronal sections at E14.5 (**b**), E17.5 (**c**), P0 (**d**–**g**) and P5 (**h**). Widespread staining was observed in the central nervous system at E11.5, and in all brain regions, with highest levels in the layer lining cerebral ventricles at P0 (arrows in **d**–**g**). Note that no staining was found in choroid plexus (arrowheads in **b**–**d** and **h**). Scale bars represent 100 μm (**b**,**c**) and 500 μm (**d**–**h**).

targeting vector containing an internal ribosomal entry site (IRES) and the *LacZ* gene into exon 23 of the *Celsr2* gene, preserving the endogenous splice acceptor (**Supplementary Fig. 1**). RT-PCR and sequencing showed that the *Celsr2* transcript (Genbank 114050894) was interrupted at nucleotide 7,107 and extended by the *IRES-LacZ-neo* sequence (**Supplementary Table 1**; see also the partial sequence of the recombinant cDNA in **Supplementary Data**). If any truncated protein is produced, it should lack all transmembrane segments encoded by nucleotides 7,123–7,851, as well as the cytoplasmic tail (nucleotides 7,852–8,763). We analyzed neonatal brain extracts from wild-type, mutant and heterozygous mice by western blot using an anti-Celsr2 antibody[24] and an antibody against beta-galactosidase. The anti-Celsr2 antibody detected a high molecular weight band in wild-type tissue. This band was less intense in extracts from heterozygous mice, and absent in those from homozygous mice, whereas the beta-galactosidase protein was present in extracts from heterozygous and homozygous mutant mice, but not wild-type mice, confirming that *LacZ* was expressed instead of *Celsr2* (**Supplementary Fig. 1**). Using the knocked-in beta-galactosidase reporter, we monitored the expression of *Celsr2* in heterozygous mice. Consistent with published data[24–26], *Celsr2* expression was detected in all brain areas, from E11.5 to P5 (**Fig. 1a**–**h**).

Celsr2 mutant mice were viable and fertile, except for some females that had vaginal atresia. At birth, their brains showed no flagrant morphological abnormalities, suggesting that Celsr2 is not essential for cerebral embryonic development. However, progressive ventricular dilation appeared between P5 and P10, with variable severity, and became obvious in all mutant mice at P21 (**Fig. 2**). The lateral ventricles were enlarged, and the septum had an abnormal triangular shape, due to reduction of the dorsal part of the lateral septum. We did not observe any stenosis or constriction at the level of the foramen of Monro or of the aqueduct. The subcommissural organ (SCO), which is thought to be involved in non-communicating hydrocephalus, was normal and synthesized the SCO-Spondin, a component of Reissner's fibers (**Supplementary Fig. 2**). Abnormalities in the choroid plexus can lead to hydrocephalus[6]. To check whether Celsr2 could be involved in the development of the choroid plexus, we analyzed its expression by beta-galactosidase staining at different time points and did not detect any signal in the choroid plexus (**Fig. 1b–d,h**). We examined the choroid plexus by transmission electron microscopy (TEM) and immunofluorescence with acetylated tubulin antibodies and found no difference between *Celsr2* mutants and control littermates (**Supplementary Fig. 3**).

In contrast, expression of *Celsr2* was very high in cells lining all cerebral ventricles and the central canal of the spinal cord (**Fig. 1d**–**g**), which differentiate into ependymal cells. To assess whether loss of Celsr2 function affects ependymal differentiation, we used immunofluorescence to examine the ependymal markers S100, CD24 and vimentin[27–29] (**Fig. 3** and **Supplementary Fig. 4**). At P0, none of the three markers was expressed in cells in the ventricular zone that were destined to form the prospective ependymal layer. At P5, we detected S100, CD24 and vimentin immunoreactivity in ependymal cells lining the septal ventricular surface in control (**Supplementary Fig. 4**) and *Celsr2*-deficient samples (**Supplementary Fig. 4**). At P10 and P21, we found S100 and CD24 in ependymal cells all around the lateral ventricles (septal, striatal and cortical surfaces), and saw no difference between controls and *Celsr2*$^{-/-}$ mutants (**Fig. 3a**,**b**,**d**,**e** and **Supplementary Fig. 4**). Similarly, vimentin was expressed in ependymal cells and, even though the signal was higher in *Celsr2* mutant mice than in controls, we found no difference in the number of vimentin-positive cells (**Fig. 3g**,**h** and **Supplementary Fig. 4**). These results rule out the possibility that hydrocephalus could be due to defective differentiation of ependymal cells in *Celsr2*-deficient mice.

The migration of young neurons, generated in the subependymal zone (SEZ) of the mature brain, depends on cerebrospinal fluid flow and is altered in hydrocephalic Tg737 mice (ref. 30). To study the relationship between hydrocephalus and neurogenesis in the SEZ, we performed immunofluorescence using doublecortin (Dcx, a marker of neuroblasts (A cells)), and GFAP (a marker of B1 cells)[27–29]. Labeling for Dcx and GFAP was slightly higher in *Celsr2* mutant mice than in controls (**Supplementary Fig. 4**).

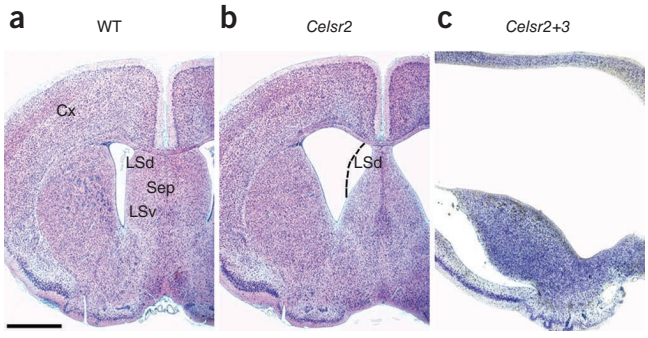

Figure 2 *Celsr2* and *Celsr2+3* mutant mice display hydrocephalus. (**a**–**c**) Nissl-stained coronal sections from wild-type (WT, left), *Celsr2* (middle) and *Celsr2+3* (right) mice at P21. Combined inactivation of *Celsr2* and *Celsr3* in ependymal cells results in severe hydrocephalus and extreme thinning of the cerebral cortex and basal forebrain (**c**). Cx, cortex; LSd, dorsal part of lateral septum; LSv, ventral part of lateral septum; Sep, septum. Scale bar represents 1 mm.

© 2010 Nature America, Inc. All rights reserved.

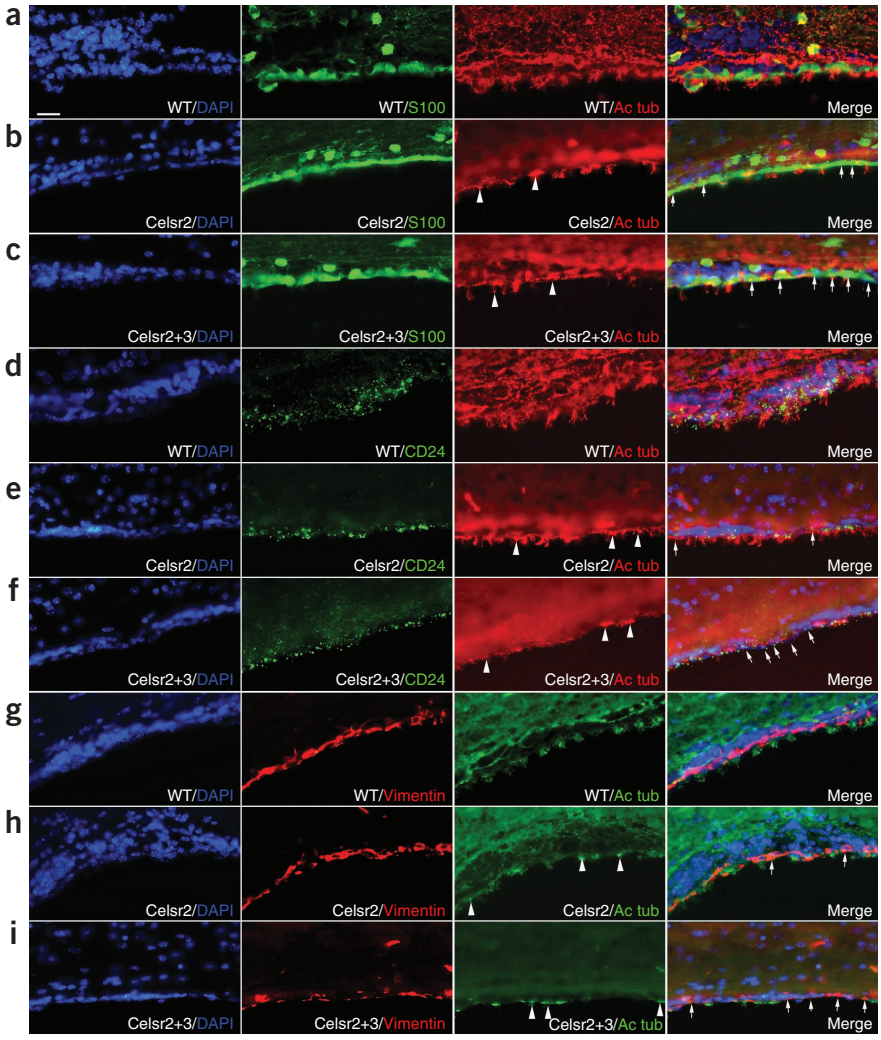

Figure 3 Ependymal cilia abnormalities in *Celsr2* and *Celsr2+3* mutant mice. (**a**–**i**) P21 brain sections were stained with DAPI (left), and by immunofluorescence for ependymal markers (second column) S100 (**a**–**c**), CD24 (**d**–**f**) and vimentin (**g**–**i**) and for acetylated alpha tubulin (third column). In *Celsr2* and *Celsr2+3* samples, ependymal cells show many ciliary defects, including shorter cilia and reduced number of cilia per cell (arrowheads), as well as absence of cilia (arrows). Scale bar represents 20 μm.

Ciliary defects in *Celsr2* mutant mice

As *Celsr2* was highly expressed in the ependymal layer (**Fig. 1d**–**g**), and impaired cilia function is a prevalent cause of hydrocephalus[6,7], we investigated ependymal cilia at P21 in the lateral ventricles by double staining with the cilia marker acetylated alpha tubulin and the ependymal markers S100, CD24 and vimentin (**Fig. 3**). Compared to wild–type mice, the number of cilia and ciliary tufts was clearly reduced in *Celsr2*$^{-/-}$ mice, in which many ependymal cells labeled by S100, CD24 or vimentin had shorter and/or fewer cilia, and sometimes no cilia at all (**Fig. 3**).

These results indicate that some cilia fail to form, or form normally and then degenerate in *Celsr2*-deficient mice. To distinguish between these possibilities, we studied cilia development at different stages with scanning electron microscopy (SEM; **Fig. 4**). In newborn (P0) wild-type animals, we found only one primary cilium (**Fig. 4a**). Tufts of cilia appeared around P5, and increased gradually in number, in a caudal-to-rostral gradient, during the first postnatal week (**Fig. 4b**,**c**), to reach their mature density at P10 (**Fig. 4d**)[31]. At this stage, there were fewer cilia tufts in *Celsr2*$^{-/-}$ mice (**Fig. 4e**) than in wild–type mice. Some mutant cells had stunted cilia (**Fig. 4e**) and others had a reduced number of cilia (arrowheads). At the end of maturation (P21), cilia abnormalities were arresting. Whereas the mean number of cilia tufts in wild-type mice was 15.8 per mm^2, and all pointed approximately in the same direction (**Fig. 4j**), the density of cilia tufts dropped to 6.7 per mm^2 in *Celsr2*-deficient mice, and their orientation was less uniform, with tufts from adjacent cells occasionally pointing in opposite directions (**Fig. 4k**). To quantify variations in the orientation of cilia tufts, we used SEM montages and plotted mean tuft orientation in cells with clearly identifiable tufts located in comparable areas of lateral ventricles in wild-type (439 cells) and *Celsr2* mutant mice (464 cells). The mean orientation was arbitrarily set to zero. Using circular statistics (Oriana program) we found that mutant ependymal cells had a wider distribution of tuft orientations than the wild-type cells ($P < 0.001$, Watson U^2 test; **Fig. 4l**,**m**). Together, these results show that cilia fail to form normally in *Celsr2* mutant mice, and that residual cilia tufts display abnormal organization at the end of maturation.

Celsr2 mutation affects cilia at the single-cell level

To study the effects of *Celsr2* inactivation on cilia development at the individual cell level, we used TEM in sections cut tangentially to the surface of the lateral ventricle, and examined the orientation of basal feet (**Fig. 5**). These structures extend laterally to basal bodies, point to the effective stroke of cilia beats[32,33] and are considered a landmark of cilia polarity[34]. In wild–type cells (**Fig. 5a**), only 8.5% of basal feet showed divergent orientation with respect to their neighbors (82 basal feet from 15 cells were examined; in 10 cells, all basal feet had uniform orientation; in the 5 others, 1 or 2 basal feet per cell showed divergent orientation). In *Celsr2* mutant cells (**Fig. 5b**), 31.8% of the basal feet deviated from the common orientation (47 out of 148 basal feet examined in 14 cells; each cell had at least one basal foot with divergent orientation). Inasmuch as some mutant cilia degenerated prematurely or did not develop at all (**Fig. 5e**) and were thus not considered, the disorganization of basal feet in *Celsr2* mutants is probably underestimated.

During assembly of motile cilia, basal bodies form deep in the cytoplasm and are transported to the apical surface by actin-dependent mechanisms[33,35,36]. To study how *Celsr2* inactivation influences ependymal ciliogenesis, we took sections perpendicular to the ventricular surface to examine by TEM the position of basal bodies relative to the apical surface of ependymal cells at P10. In wild-type samples, basal bodies formed a single row just beneath the apical surface (**Fig. 5d**). By contrast, procentrioles and basal bodies, together with densely osmiophilic profiles that probably correspond to deuterosomes, were found at deeper, more basal levels in *Celsr2* mutant cells (**Fig. 5e**). To quantify these differences,

© 2010 Nature America, Inc. All rights reserved.

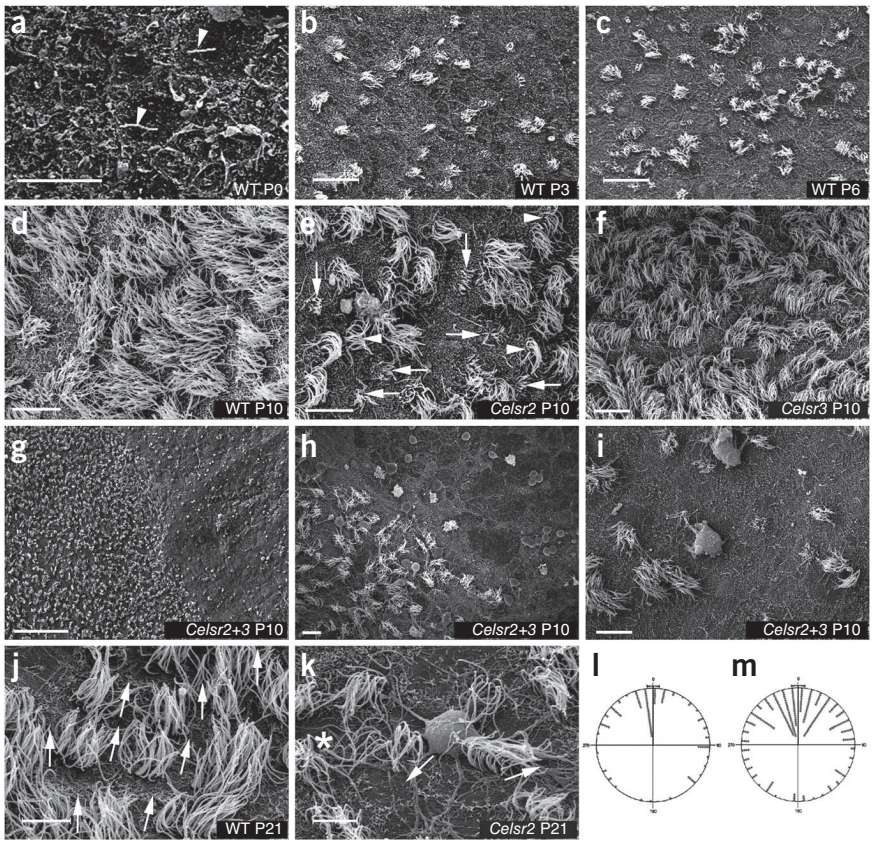

Figure 4 Ciliogenesis is altered in *Celsr2* and *Celsr2+3* deficient mice. (**a**–**k**) SEM micrographs of ependymal cells lining the roof of lateral ventricles at P0 (**a**, arrowheads show monocilia), P3 (**b**), P6 (**c**), P10 (**d**–**i**) and P21 (**j**,**k**). Cilia develop progressively after birth and reach maturity by P10. At this stage, the number of cilia tufts is reduced and cilia have many morphological abnormalities in *Celsr2* (**e**) and *Celsr2+3* (**g**–**i**) mutants as compared to wild-type (**d**) and *Celsr3* mutants (**f**). Arrows show shorter cilia, and arrowheads cilia tufts with reduced number of cilia. In the mature brain, individual cilia converge to a common orientation in the wild type (arrows in **j**), but cilia tufts of mutant mice (**k**) are less regularly oriented and, in some cases, individual cilia in a given cell do not point in the same direction (asterisks). (**l**,**m**) Dispersion of cilia tuft orientation around the mean in wild-type (**l**) and *Celsr2* mutant mice (**m**). Scale bars represent 5 μm (**a**,**j**,**k**), 10 μm (**d**–**f**, **h**–**i**), 20 μm (**b**,**c**) and 100 μm (**g**).

we measured the distance between basal bodies and the apical surface and calculated the proportion of embedded basal bodies (defined as basal bodies located below the first row, more than 500 nm from the surface). In *Celsr2*$^{-/-}$ mice, 54% of basal bodies were embedded versus 5% in wild type mice (**Fig. 5g**; X^2 test, $P < 0.001$). Most embedded basal bodies were not associated with ciliary shafts. However, fully formed cilia were occasionally seen deep in the cytoplasm (**Fig. 5h**). Presumably, ectopic cilia and embedded basal bodies are fated to premature degeneration, which might account for the reduced density of cilia in adult *Celsr2* mutant ependymal cells.

Celsr2 mutation impairs cilia function

In rodents, mutations that affect ciliary motility lead to hydrocephalus[5–8,37]. The ultrastructure of residual *Celsr2* mutant cilia were unremarkable and displayed the typical 9+2 structure of motile cilia (**Supplementary Fig. 5**). This indicated that *Celsr2* mutation has no direct effect on the axoneme structure and raised the question of the motility of cilia in *Celsr2* mutants. To investigate this, we prepared brain slices from 12-day-old animals and recorded cilia movement with a high-speed camera. We found two classes of movement in wild–type mice. One movement is more dynamic than the other, and reminiscent of seaweed drifting on restless waves. The other is a smaller motion that resembles a

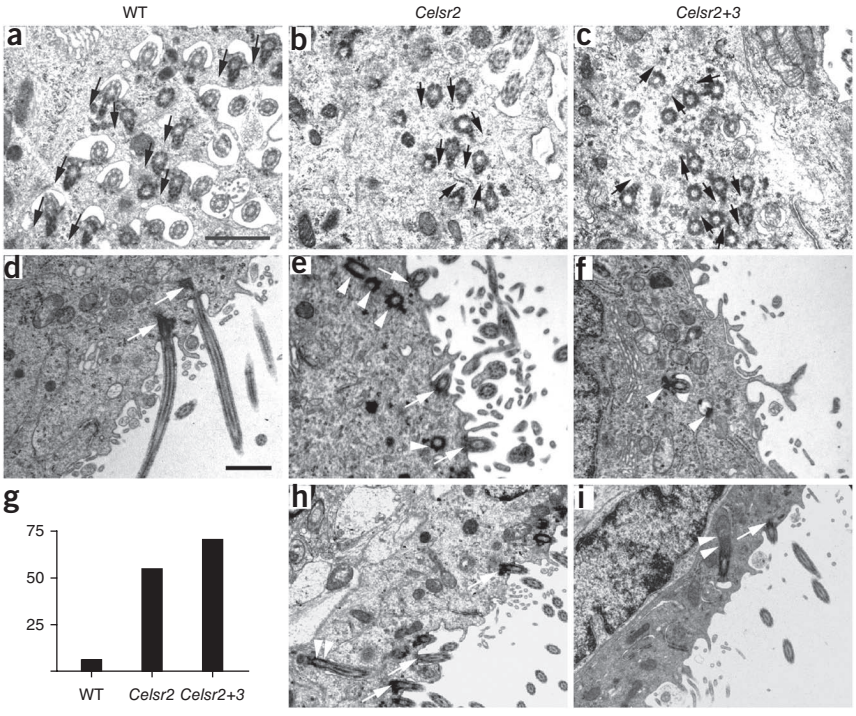

Figure 5 Inactivation of *Celsr2* and *3* affects polarization and apical positioning of cilia. (**a**–**c**) TEM analysis of tangential sections of ependymal cells from wild-type (**a**), *Celsr2* (**b**) and *Celsr2+3* animals (**c**). Arrows indicate the orientation of basal feet which show dispersed orientations in mutants. (**d**–**f**,**h**,**i**) Ependymal cells in radial sections, from wild-type (**d**), *Celsr2* (**e**,**h**) and *Celsr2+3* (**f**,**i**) mice. Arrows point to normally positioned basal bodies, arrowheads to embedded basal bodies and double arrowheads to ectopic cilia. (**g**) Graph showing the proportion of basal bodies with abnormal apicobasal position. Scale bars represent 500 nm (**a**, applies to **b**–**c**) and 1 μm (**d**, applies to **e**,**f**,**h**,**i**).

© 2010 Nature America, Inc. All rights reserved.

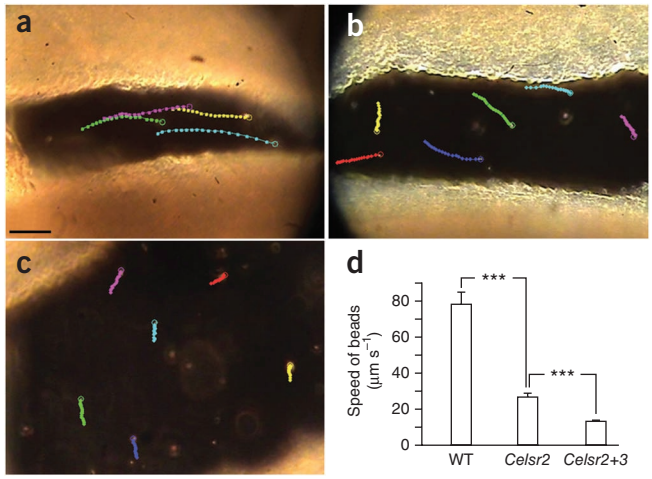

Figure 6 *Celsr2* and *Celsr2+3* deficiency affects fluid flow. Latex beads were added to brain slices from P8 mice and their movement in the lateral ventricle was recorded with a video camera. Movies were fragmented and sequential images were analyzed using Retrac 2 software. Each bead was tracked for 720 ms and the time between two dots is 40 ms. Circles indicate track end-points. (**a**–**d**) In the wild type (**a**), bead motion was uniform and trajectories formed almost parallel lines. In *Celsr2* (**b**) and *Celsr2+3* (**c**) mutants, tracks were shorter than in the controls and beads moved in divergent directions (Watson U^2 test, $P < 0.05$; **Supplementary Table 2**). The speed was calculated for each genotype and is shown as mean ± s.e.m. in **d**; $***P < 0.0001$. Scale bar represents 20 μm.

'wiggling pigeon's neck'. Both classes were found in *Celsr2* mutant cells that harbored intact cilia, indicating that cilia movements were not grossly affected by Celsr2 deficiency (**Supplementary Movies 1**–**4**).

Could the reduced number of cilia and cilia tufts result in inefficient CSF dynamics despite the preserved cilia beat at the single cell level? To address this question, we studied the flow generated by cilia beats in lateral ventricles in vibratome slices, taken from mice aged between P0 and P21. Ependymal cilia were beating from P5 onwards, but they generated a significant flow only from P8 (**Fig. 6** and **Supplementary Movie 5**). When latex beads were added to the medium of wild-type slices at P7–10 (**Fig. 6a**; $n = 13$), their movement was consistently directed from the caudal to the rostral pole of the lateral ventricles (see Online Methods), with a mean bead velocity of 78.3 ± 35.6 (SD) μm s^{-1}. In *Celsr2*-deficient slices (**Fig. 6b**; $n = 19$), the overall movement of beads was slower and less clearly directed toward the rostral pole than in the wild type, and the mean bead velocity was 26.6 ± 9.7 μm s^{-1}. Frequently, beads showed a circling movement without any clear resultant displacement along the rostrocaudal axis (**Supplementary Movie 5**). Both directions and velocities, compared respectively using Watson U^2 (**Supplementary Table 2**) and Student's *t*-test (**Fig. 6d**), were significantly different between the two genotypes. Although the size of the ventricle could affect the speed of bead movement, our data indicate that inactivation of *Celsr2* impairs the efficiency of cilia beats, which could compromise CSF dynamics and thereby contribute to hydrocephalus.

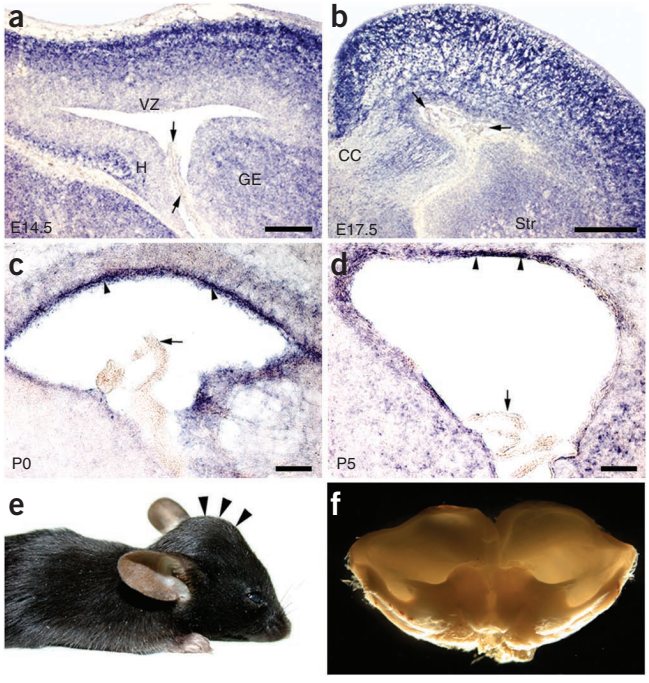

Celsr2 and *3* have redundant functions in ciliogenesis

Celsr3 expression is not detected in ventricular zones during embryonic development[24,25] (**Fig. 7a**,**b**), but is initiated postnatally in cells that line the lateral ventricles, when they become postmitotic and start differentiating into ependymal cells[25] (**Fig. 7c**,**d**). We have evidence that *Celsr2* and *Celsr3* have redundant functions in neuronal migration and axon guidance, indicating that they might similarly cooperate in ependymal ciliogenesis. To test this possibility, we studied the ependymal cells of lateral ventricles in double *Celsr2*/*Celsr3* mutant mice. Constitutive *Celsr3* mutant mice die at P0 (ref. 19). Therefore, we produced *Celsr3*|*Emx1* mice, in which Cre is expressed from the *Emx1* promoter and deletes *loxP*-flanked *Celsr3* in the *Emx1*-expressing dorsal telencephalon, including the ependymal layer in the roof of lateral ventricles[23]. In these mice, referred to as '*Celsr3*', cilia were indistinguishable from those in wild-type cells (**Fig. 4d**,**f**). The density of cilia tufts was 15.6 per mm^2, compared with 15.8 per mm^2 for the wild type, confirming that mutation of *Celsr3* alone did not perturb ependymal cilia development. However, when regional *Celsr3* inactivation was combined with deficiency of *Celsr2* in *Celsr2*$^{-/-}$/*Celsr3*|*Emx1* mice, referred to as '*Celsr2+3*', a severe hydrocephalus appeared from P5. The hydrocephalus was much more pronounced than in *Celsr2* mutant animals (**Fig. 2b**,**c**). Even though *Celsr3* is ablated only in *Emx1*-expressing ependyma, this led to extreme thinning of the cerebral cortex, with formation of a discontinuity in the dorsal hemisphere, and death of animals around weaning time (**Fig. 7e**,**f**). The number of Dcx- and GFAP-positive cells was higher in *Celsr2+3* mutants than in controls (**Supplementary Fig. 4**). Immunofluorescence analysis of S100, CD24 and vimentin indicated that ependymal cells differentiated normally (**Supplementary Fig. 4**) and persisted in the mature mutant brain (**Fig. 3c**,**f**,**i**), although their shape was stretched and some cells might have degenerated because of increased pressure, as reflected by vimentin immunoreactivity (**Fig. 3i**). Large areas of the

Figure 7 Combined mutation of *Celsr2* and *Celsr3* causes lethal hydrocephalus. (**a**–**d**) Coronal sections hybridized with *Celsr3* digoxigenin-labeled probe. *Celsr3* is not expressed in the ventricular zones at E14.5 (**a**), but is turned on postnatally in cells of the prospective ependymal layer (**c**,**d**, arrowheads). Note the absence of *Celsr3* transcript in the choroid plexus (arrows in **a**–**d**). (**e**) *Celsr2+3* mutant mice have a dome-like appearance of the head caused by hydrocephalus, and their brains (**f**) show extreme thinning of cerebral cortex and holes in telencephalic walls. CC: corpus callosum; GE: ganglionic eminence; H: hippocampus; Str: striatum; VZ: ventricular zone. Scale bar represents 200 μm.

© 2010 Nature America, Inc. All rights reserved.

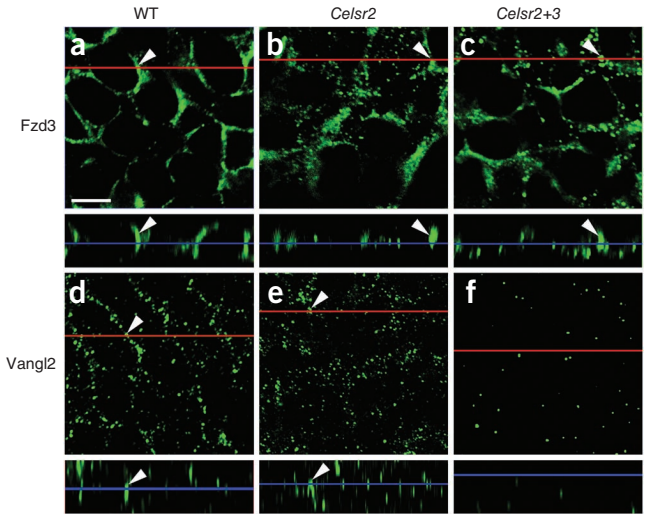

Figure 8 The cellular distribution of Fzd3 and Vangl2 is perturbed in *Celsr2* and *Celsr2+3* mice. (**a**–**f**) Confocal immunofluorescence imaging showing the cellular distribution of Fzd3 (**a**–**c**, horizontal sections in upper panels, and vertical sections in lower panels) and Vangl2 (**d**–**f**), in the ventricular zone at P5. The polygonal pattern that reflects localization of Fzd3 (**a**) and Vangl2 (**d**) at the lateral plasma membrane in normal mice (arrowheads) is modified in *Celsr2* (**b**,**e**) and *Celsr2+3* (**c**,**f**) mutants. The Z sections (rows 2 and 4) are at the level of red lines in horizontal sections (rows 1 and 3), which were recorded at the position of blue lines in vertical sections. Scale bar represents 5 μm.

dorsal lateral ventricles were completely devoid of cilia (**Fig. 4g**–**i**), preventing any accurate estimation of cilia tuft density. These cilia-free zones persisted until death, indicating defective rather than delayed ciliogenesis. In cells with residual cilia, the percentage of basal feet with abnormal orientation reached 43.16% (60 of 139 scored basal feet; **Fig. 5c**). These abnormalities were comparable to those reported in mice with defective cilia motility, such as Hydin-deficient mice[7]. We found that 70% of the basal bodies were embedded in the basal cytoplasm (**Fig. 5f**,**g**). Ectopic cilia had a tilted configuration and their tips were not oriented apically, contrasting with the upright alignment of apical cilia in wild-type and ectopic cilia in *Celsr2* mutant cells (**Fig. 5i**). When latex beads were added to freshly prepared brain slices from *Celsr2+3* mice (**Fig. 6c**; $n = 2$), they drifted very slowly along different directions in the enlarged ventricle, with an estimated velocity of 13.0 ± 4.2 μm s^{-1} versus 78.3 ± 35.6 μm s^{-1} for the wild type. This difference was statistically significant using the Watson U^2 test (**Supplementary Table 2**) and Student's *t*-test (**Fig. 6d**).

Emx1-Cre is expressed not only in ependyma but also in cortical glutamatergic neurons and glial cells. To confirm that the effects observed were due to Celsr3 deficiency in the ependyma, we produced double mutant *Celsr2*$^{-/-}$/*Celsr3|Nex* mice, in which *Celsr3* is inactivated in cortical neurons but not in ependyma[38]. The brains of these mice were indistinguishable from those in *Celsr2*$^{-/-}$ animals ($n = 5$), showing that the contribution of *Celsr3* to the double mutant phenotype is probably due to its expression in ependymal cells.

Fzd3 and Vangl2 distribution is altered in *Celsr* mutants

Studies in the skin showed that PCP signaling is essential for hair follicle polarization and orientation[15–17]. Celsr1 and Vangl2 form physical complexes *in vitro*, and Celsr1 is required for the correct targeting of Vangl2 and Fzd6 to the plasma membrane[17]. To gain insight into the mechanisms of action of Celsr2 and Celsr3, and to assess whether their function could be mediated by PCP, we studied the distribution of Fzd3 and Vangl2, two key components of the PCP pathway that are expressed in ependymal cell precursors[14,39,40] (**Fig. 8**). In wild type brains at P5, Fzd3 and Vangl2 signals displayed polygonal patterns, restricted to the lateral membrane, with a continuous (Fzd3) or punctate distribution (Vangl2; **Fig. 8a**,**d**). In *Celsr2*$^{-/-}$ tissue, Fzd3 and especially Vangl2 were only partially targeted to the cell membrane. Rather, more signal was associated with intracellular vesicles (**Fig. 8b**,**e**). In *Celsr2+3* double mutants, the impaired distribution of Fzd3 was even more evident, whereas Vangl2 was downregulated (**Fig. 8c**,**f**). The restricted polygonal pattern upon labeling of the junctional protein ZO-1 was fully preserved in *Celsr2* and *Celsr2+3* mutants, showing that the abnormal distribution of Vangl2 and Fzd3 was not secondary to defective junction organization (**Supplementary Fig. 6**).

DISCUSSION

Using *in vivo* approaches in mice, we found that *Celsr2* and *Celsr3*, two murine orthologs of the core PCP gene *Flamingo* in *Drosophila*, are key regulators of ciliogenesis in the ependyma, and that their inactivation leads to lethal hydrocephalus. In *Celsr2* and *Celsr2+3* mutant ependyma, cilia never develop in normal numbers and show abnormalities in their morphology, position and planar organization. Ciliary basal feet are disoriented, and basal bodies and cilia assemble ectopically deep in the cytoplasm. These defects do not primarily affect cilia motility; however, they alter ependymal function, leading to ventricular dilation. The lateral plasma membrane localization of Vangl2 and Frizzled3, two established PCP proteins, is disrupted in ependymal cell precursors in *Celsr2* and *Celsr2+3* mutant mice, providing a strong indication that Celsr2 and Celsr3 regulate ciliogenesis through PCP signaling.

Previous studies in frog larval epidermal cells provided the first evidence of a link between PCP signaling and cilia development. In these cells, morpholino knockdown of *Inturned*, *Fuzzy* and *Disheveled1–3* affect cilia polarity and ciliogenesis by preventing normal docking of basal bodies to the apical cytoplasm[21,22]. Although these studies indicate a relationship between ciliogenesis and PCP signaling, *Inturned* and *Fuzzy* are not considered bona fide core PCP genes, and, besides PCP, *Disheveled1–3* also regulate canonical and non-canonical Wnt signaling. Moreover, being near tetraploid, *Xenopus laevis* cells might express PCP gene orthologs other than those that are identified in *Xenopus tropicalis* and whose sequences are used for morpholino design. In mice, mutations in genes that encode proteins implicated in cilia structure or development, such as *Bbs1*, *Bbs4* and *Ift888*, affect the 'V shaped' orientation of actin stereocilia bundles at the surface of inner ear cells, an organization that is governed by the directed growth of a monocilium during development[39,41]. This phenotypic trait is typically found in mice with mutations in the PCP genes *Celsr1*, *Frizzled3*, *Frizzled6* and *Vangl2* (refs. 11,13,14). Furthermore, conditional inactivation of the ciliary gene *Kif3a* in neural progenitors and radial glia affects the orientation of ciliary basal feet and planar polarity of ependymal cells[42]. These data suggest that the link between PCP and ciliogenesis, described in amphibian epidermal cells, is conserved in mammals. Our observations that the core PCP genes *Celsr2* and *Celsr3* are essential for the correct positioning of cilia at the apical surface of ependymal cells, for cilia function as well as for CSF dynamics, extend and clarify this view.

Presumably, PCP signals act on the cytoskeletal machinery that is required to assemble cilia at the cell surface, a mechanism highly reminiscent of that involved in the growth of the actin shafts of hairs in *Drosophila* wing cells[43]. That PCP signaling acts upstream from

© 2010 Nature America, Inc. All rights reserved.

cilium assembly is also supported by observations that PCP proteins are normally distributed in cochlear cells in mice with mutation of the 'ciliary gene' *Ift888* (ref. 39). Factors that regulate apical basal body docking remain poorly understood. Our observations that cilia can form deep in the cytoplasm in *Celsr2* and *Celsr2+3* mutant ependymal cells and that ectopic basal bodies can still serve as seeds for cilia formation indicate that apical docking is not absolutely required for cilia assembly *per se*. Studies of ciliogenesis in the quail oviduct showed that localization of basal bodies to the apical cell domain depends on actin dynamics[35]. In line with this, ciliogenesis is defective in *Foxj1* mutant mice, owing to abnormal basal body anchoring to the actin-based apical cytoskeleton and to failure of RhoA-mediated apical actin enrichment[44–47]. The hypothesis that PCP signaling regulates the apical actin network formation that is required for docking of basal bodies and normal ciliogenesis predicts that mutations in other genes that control PCP in mice should similarly lead to cilia dysfunction and hydrocephalus. Unfortunately, unlike *Celsr2* mutants, mice with mutations in other PCP genes, such as *Frizzled3* and *6* (ref. 40) and *Vangl2* (ref. 12) all die perinatally, before ependymal cilia develop. The generation of conditional mutant mice for PCP gene orthologs would provide additional tools to address these issues. In addition to defective docking, we also find impairment of the planar organization of cilia tufts in mature *Celsr* mutant ependymal layers. This phenotype could reflect a direct effect of *Celsr* mutations, but it might also be a consequence of disturbed CSF flow[34] in these hydrocephalic mice.

Finally, our findings underscore the role of PCP signaling in ependymal function and hydrocephalus. In man, CSF flow is commonly ascribed to a pressure gradient, generated by blood pulsations, between the sites of production and absorption. In contrast to rodents, cilia beats are usually not considered a key determinant of human CSF dynamics, nor a relevant pathophysiological factor of hydrocephalus[48]. Our results add to a growing body of evidence that the impact of cilia on CSF dynamics is extremely important in rodents and probably not negligible in man, and invite additional scrutiny of ependyma and cilia function in patients with communicating hydrocephalus. Abnormalities of cilia are also associated with cystic pathology in the kidney, liver and pancreas[1,49]. PCP genes such as *Celsr1* and *2*, *Disheveled1* and *2*, *Frizzled3* and *Vangl1* and *2* are expressed in these organs[24,50], indicating that PCP signaling might be involved in the polarity and function of their cilia, in both normal and pathological conditions.

METHODS

Methods and any associated references are available in the online version of the paper at http://www.nature.com/natureneuroscience/.

Note: Supplementary information is available on the Nature Neuroscience website.

ACKNOWLEDGMENTS

We thank K. Jones for *Emx1-Cre* mice, G. Meyer for the antibody to SCO-spondin, and K.-A. Nave for NEX-Cre mice. We also thank V. Bonte, I. Lambermont and E. Paitre for technical assistance and M.F. Boulanger, Y. Houbion, M.-J. Vertez and R. Vigneron for help with electron microscopy. This work was supported by grants from the Actions de Recherches Concertées (ARC-186), FRFC 2.4504.01, FRSM 3.4501.07, Interuniversity Poles of Attraction (SSTC, PAI p6/20), the Fondation médicale Reine Elisabeth, the Wallonne and Bruxelloise régions from Belgium and from the Japan Science and Technology Corporation. F.T. is a research associate at the Belgian Fonds National de la Recherche Scientifique.

AUTHOR CONTRIBUTIONS

F.T. characterized the *Celsr2* mutant allele, studied Celsr2 and Celsr3 expression and carried out histological and immunofluorescence studies; Y.Q. performed SEM and TEM with the help of Y.P.; L.Z. and J.L. studied cilia function in brain slices; K.K. monitored cilia beats and analyzed data with D.S. and T.F.; M.M. provided the Vangl2 antibody and commented on the manuscript; D.S. and P.C. helped with the confocal microscopy and commented on the manuscript; T.U. analyzed the ciliary beat data, provided the Celsr2 antibody and commented on the manuscript; F.T. and A.M.G. designed research, analyzed data and wrote the manuscript.

COMPETING FINANCIAL INTERESTS

The authors declare no competing financial interests.

Published online at http://www.nature.com/natureneuroscience/.
Reprints and permissions information is available online at http://www.nature.com/reprintsandpermissions/.

1. Davenport, J.R. & Yoder, B.K. An incredible decade for the primary cilium: a look at a once-forgotten organelle. *Am. J. Physiol. Renal Physiol.* **289**, F1159–F1169 (2005).
2. Marshall, W.F. & Kintner, C. Cilia orientation and the fluid mechanics of development. *Curr. Opin. Cell Biol.* **20**, 48–52 (2008).
3. Salathe, M. Regulation of mammalian ciliary beating. *Annu. Rev. Physiol.* **69**, 401–422 (2007).
4. Voronina, V.A. *et al.* Inactivation of Chibby affects function of motile airway cilia. *J. Cell Biol.* **185**, 225–233 (2009).
5. Ibañez-Tallon, I. *et al.* Dysfunction of axonemal dynein heavy chain Mdnah5 inhibits ependymal flow and reveals a novel mechanism for hydrocephalus formation. *Hum. Mol. Genet.* **13**, 2133–2141 (2004).
6. Banizs, B. *et al.* Dysfunctional cilia lead to altered ependyma and choroid plexus function, and result in the formation of hydrocephalus. *Development* **132**, 5329–5339 (2005).
7. Lechtreck, K.F., Delmotte, P., Robinson, M.L., Sanderson, M.J. & Witman, G.B. Mutations in Hydin impair ciliary motility in mice. *J. Cell Biol.* **180**, 633–643 (2008).
8. Davy, B.E. & Robinson, M.L. Congenital hydrocephalus in hy3 mice is caused by a frameshift mutation in Hydin, a large novel gene. *Hum. Mol. Genet.* **12**, 1163–1170 (2003).
9. Simons, M. & Mlodzik, M. Planar cell polarity signaling: from fly development to human disease. *Annu. Rev. Genet.* **42**, 517–540 (2008).
10. Strutt, D.I., Weber, U. & Mlodzik, M. The role of RhoA in tissue polarity and Frizzled signaling. *Nature* **387**, 292–295 (1997).
11. Wang, Y. & Nathans, J. Tissue/planar cell polarity in vertebrates: new insights and new questions. *Development* **134**, 647–658 (2007).
12. Kibar, Z. *et al.* Ltap, a mammalian homolog of *Drosophila* Strabismus/Van Gogh, is altered in the mouse neural tube mutant Loop-tail. *Nat. Genet.* **28**, 251–255 (2001).
13. Curtin, J.A. *et al.* Mutation of Celsr1 disrupts planar polarity of inner ear hair cells and causes severe neural tube defects in the mouse. *Curr. Biol.* **13**, 1129–1133 (2003).
14. Montcouquiol, M. *et al.* Asymmetric localization of Vangl2 and Fz3 indicate novel mechanisms for planar cell polarity in mammals. *J. Neurosci.* **26**, 5265–5275 (2006).
15. Ravni, A., Qu, Y., Goffinet, A.M. & Tissir, F. Planar cell polarity cadherin Celsr1 regulates skin hair patterning in the mouse. *J. Invest. Dermatol.* **129**, 2507–2509 (2009).
16. Guo, N., Hawkins, C. & Nathans, J. Frizzled6 controls hair patterning in mice. *Proc. Natl. Acad. Sci. USA* **101**, 9277–9281 (2004).
17. Devenport, D. & Fuchs, E. Planar polarization in embryonic epidermis orchestrates global asymmetric morphogenesis of hair follicles. *Nat. Cell Biol.* **10**, 1257–1268 (2008).
18. Shima, Y. *et al.* Opposing roles in neurite growth control by two seven-pass transmembrane cadherins. *Nat. Neurosci.* **10**, 963–969 (2007).
19. Tissir, F., Bar, I., Jossin, Y. & Goffinet, A.M. Protocadherin Celsr3 is crucial in axonal tract development. *Nat. Neurosci.* **8**, 451–457 (2005).
20. Wang, Y., Thekdi, N., Smallwood, P.M., Macke, J.P. & Nathans, J. Frizzled-3 is required for the development of major fiber tracts in the rostral CNS. *J. Neurosci.* **22**, 8563–8573 (2002).
21. Park, T.J., Mitchell, B.J., Abitua, P.B., Kintner, C. & Wallingford, J.B. Dishevelled controls apical docking and planar polarization of basal bodies in ciliated epithelial cells. *Nat. Genet.* **40**, 871–879 (2008).
22. Park, T.J., Haigo, S.L. & Wallingford, J.B. Ciliogenesis defects in embryos lacking inturned or fuzzy function are associated with failure of planar cell polarity and Hedgehog signaling. *Nat. Genet.* **38**, 303–311 (2006).
23. Zhou, L. *et al.* Early forebrain wiring: genetic dissection using conditional Celsr3 mutant mice. *Science* **320**, 946–949 (2008).
24. Shima, Y. *et al.* Differential expression of the seven-pass transmembrane cadherin genes Celsr1–3 and distribution of the Celsr2 protein during mouse development. *Dev. Dyn.* **223**, 321–332 (2002).
25. Tissir, F., De-Backer, O., Goffinet, A.M. & Lambert de Rouvroit, C. Developmental expression profiles of Celsr (Flamingo) genes in the mouse. *Mech. Dev.* **112**, 157–160 (2002).
26. Formstone, C.J. & Little, P.F. The flamingo-related mouse Celsr family (Celsr1–3) genes exhibit distinct patterns of expression during embryonic development. *Mech. Dev.* **109**, 91–94 (2001).

© 2010 Nature America, Inc. All rights reserved.

27. Town, T. *et al.* The stumpy gene is required for mammalian ciliogenesis. *Proc. Natl. Acad. Sci. USA* **105**, 2853–2858 (2008).
28. Mirzadeh, Z., Merkle, F.T., Soriano-Navarro, M. & Garcia-Verdugo, J.M. & Alvarez-Buylla, A. Neural stem cells confer unique pinwheel architecture to the ventricular surface in neurogenic regions of the adult brain. *Cell Stem Cell* **3**, 265–278 (2008).
29. Danilov, A.I. *et al.* Ultrastructural and antigenic properties of neural stem cells and their progeny in adult rat subventricular zone. *Glia* **57**, 136–152 (2009).
30. Sawamoto, K. *et al.* New neurons follow the flow of cerebrospinal fluid in the adult brain. *Science* **311**, 629–632 (2006).
31. Spassky, N. *et al.* Adult ependymal cells are postmitotic and are derived from radial glial cells during embryogenesis. *J. Neurosci.* **25**, 10–18 (2005).
32. Boisvieux-Ulrich, E. & Sandoz, D. Determination of ciliary polarity precedes differentiation in the epithelial cells of quail oviduct. *Biol. Cell* **72**, 3–14 (1991).
33. Dawe, H.R., Farr, H. & Gull, K. Centriole/basal body morphogenesis and migration during ciliogenesis in animal cells. *J. Cell Sci.* **120**, 7–15 (2007).
34. Mitchell, B., Jacobs, R., Li, J., Chien, S. & Kintner, C. A positive feedback mechanism governs the polarity and motion of motile cilia. *Nature* **447**, 97–101 (2007).
35. Boisvieux-Ulrich, E., Laine, M.C. & Sandoz, D. Cytochalasin D inhibits basal body migration and ciliary elongation in quail oviduct epithelium. *Cell Tissue Res.* **259**, 443–454 (1990).
36. Boisvieux-Ulrich, E., Laine, M.C. & Sandoz, D. *In vitro* effects of benzodiazepines on ciliogenesis in the quail oviduct. *Cell Motil. Cytoskeleton* **8**, 333–344 (1987).
37. Marshall, W.F. The cell biological basis of ciliary disease. *J. Cell Biol.* **180**, 17–21 (2008).
38. Goebbels, S. *et al.* Genetic targeting of principal neurons in neocortex and hippocampus of NEX-Cre mice. *Genesis* **44**, 611–621 (2006).
39. Jones, C. *et al.* Ciliary proteins link basal body polarization to planar cell polarity regulation. *Nat. Genet.* **40**, 69–77 (2008).
40. Wang, Y., Guo, N. & Nathans, J. The role of Frizzled3 and Frizzled6 in neural tube closure and in the planar polarity of inner-ear sensory hair cells. *J. Neurosci.* **26**, 2147–2156 (2006).
41. Ross, A.J. *et al.* Disruption of Bardet-Biedl syndrome ciliary proteins perturbs planar cell polarity in vertebrates. *Nat. Genet.* **37**, 1135–1140 (2005).
42. Mirzadeh, Z., Han, Y.G., Soriano-Navarro, M., Garcia-Verdugo, J.M. & Alvarez-Buylla, A. Cilia organize ependymal planar polarity. *J. Neurosci.* **30**, 2600–2610 (2010).
43. Wong, L.L. & Adler, P.N. Tissue polarity genes of *Drosophila* regulate the subcellular location for prehair initiation in pupal wing cells. *J. Cell Biol.* **123**, 209–221 (1993).
44. Chen, J., Knowles, H.J., Hebert, J.L. & Hackett, B.P. Mutation of the mouse hepatocyte nuclear factor/forkhead homologue 4 gene results in an absence of cilia and random left-right asymmetry. *J. Clin. Invest.* **102**, 1077–1082 (1998).
45. Brody, S.L., Yan, X.H., Wuerffel, M.K., Song, S.K. & Shapiro, S.D. Ciliogenesis and left-right axis defects in forkhead factor HFH-4-null mice. *Am. J. Respir. Cell Mol. Biol.* **23**, 45–51 (2000).
46. Pan, J., You, Y., Huang, T. & Brody, S.L. RhoA-mediated apical actin enrichment is required for ciliogenesis and promoted by Foxj1. *J. Cell Sci.* **120**, 1868–1876 (2007).
47. Gomperts, B.N., Gong-Cooper, X. & Hackett, B.P. Foxj1 regulates basal body anchoring to the cytoskeleton of ciliated pulmonary epithelial cells. *J. Cell Sci.* **117**, 1329–1337 (2004).
48. Ropper, A.H. & Brown, R.H. *Adams and Victor's Principles of Neurology* (McGraw Hill, 2005).
49. Sharma, N., Berbari, N.F. & Yoder, B.K. Ciliary dysfunction in developmental abnormalities and diseases. *Curr. Top. Dev. Biol.* **85**, 371–427 (2008).
50. Tissir, F. & Goffinet, A.M. Expression of planar cell polarity genes during development of the mouse CNS. *Eur. J. Neurosci.* **23**, 597–607 (2006).

© 2010 Nature America, Inc. All rights reserved.

ONLINE METHODS

Mutant mice. All animal procedures were carried out in accordance with European guidelines and approved by the animal ethics committee of the Université catholique de Louvain. The *Celsr2* mutant allele (*Celsr2*^{tm1Dgen}) was generated by Deltagen and *Celsr2* heterozygous mutant mice were obtained from the Jackson Laboratory. *Celsr3* and *Celsr1* mutants have been described[23].

RT-PCR. Total RNA was extracted using NucleoSpin RNA II kit (Macherey-Nagel) and converted to single-stranded cDNA using the ImProm-II reverse transcriptase (Promega) with random primer (0.5 μg ml^{-1}) in 20 μl of 1× ImProm-II buffer (6 mM $MgCl_2$, 0.5 mM each dNTP, and 2 U recombinant RNasin RNase inhibitor). For subsequent PCR amplification, cDNA samples were incubated with 500 nM of each of the sense and antisense primers and 1 U of recombinant Go Taq polymerase (Promega) in 20 μl of 1× PCR buffer.

Beta-galactosidase staining. Animals were perfused with 2% paraformaldehyde, 0.1% glutaraldehyde in phosphate-buffered saline. Dissected brains were post-fixed for 1 h at room temperature, sliced using a vibratome and stained with a solution containing 1 mg ml^{-1} X-gal, 5 mM $K_3Fe(CN)_6$, 5 mM $K_4Fe(CN)_6$ and 2 mM $MgCl_2$ in phosphate-buffered saline.

Western blot, histology and immunohistochemistry. For western blots, we used mouse antibody to beta-galactosidase (1:200, Hybridoma Bank) and mouse antibody to Celsr2 (supernatant)[24]. For histological examination, 8-μm-thick paraffin sections were stained with cresyl violet or hematoxylin and eosin (H&E). For immunohistochemistry, we used 10-μm-thick sections or 100-μm-thick vibratome slices with the following primary antibodies: rabbit antibody to SCO-spondin (1:1,000, gift from G. Meyer, Universidad de la Laguna, and E.M. Rodriguez, Universidad Austral de Chile), rabbit antibody to S100 (1:500, DakoCytomation), mouse antibody to actylated alpha tubulin (1:2,500, Sigma), mouse antibody to vimentin (1:1,000, Sigma), rat antibody to CD24 (1:500, BD Pharmigen), rabbit antibody to GFAP (1:500, Chemicon), rabbit antibody to doublecortin (1:500, Cell signaling), goat antibody to Fzd3 (1:25, R&D), rabbit antibody to Vangl2 (1:500, M.M.) and rabbit antibody to ZO-1 (1:100, Zymed). Secondary antibodies were goat antibody to mouse-AlexaFluor488 and AlexaFluor568, goat antibody to rabbit-AlexaFluor488 and AlexaFluor568, donkey antibody to goat AlexaFluor488 and chicken antibody to rat AlexaFluor488 (1:400, all from Invitrogen). Immunofluorescence was performed using standard procedures; preparations were examined with a LSM510 confocal microscope (Zeiss).

Recording and analysis of cilia beats. We observed cilia in freshly prepared, 300-μm-thick vibratome sections at P7, P8 and P10. Sections were maintained in DMEM containing 20 mM HEPES in air as described[7], or in artificial cerebrospinal fluid (ACSF: 124 mM NaCl, 3 mM KCl, 26 mM $NaHCO_3$, 2 mM $CaCl_2$, 1 mM $MgSO_4$, 1.25 mM KH_2PO_4, 25 mM glucose and 10 mM HEPES, pH 7.4) under water-saturated 95% oxygen and 5% CO_2. A maximum of 1 h elapsed between death of animals and the end of observations, and both methods yielded similar results. We added 1 μm latex beads (Sigma L2778) to the medium before video recording. Movies were fragmented into individual images corresponding to 40 ms, and beads were tracked in selected frame series using the Retrac 2 program to estimate speed and direction. Directions (30–40 tracks for each genotype) were compared using circular statistics, Watson U^2 test (Oriana program).

For high-speed recording of individual cilia beats, we used a 100× objective and Nomarski optics. Movies were acquired at 200 frames per second using a digital high-speed camera (HAS-220; Ditect) and analyzed using Move-MN software (Library Inc).

Electron microscopy. Brains were fixed by perfusion of the animal under deep anesthesia, with 2.5% glutaraldehyde in phosphate or cacodylate buffer (0.1 M, pH 7.5), and postfixed for 1 h in the same fixative. For SEM, 300–500-μm-thick horizontal slices containing the roof of the lateral ventricles were cut with a vibratome, dehydrated and prepared for observation using a Jeol 7500F scanning electron microscope. Blocs for TEM were rinsed, postfixed in osmium and embedded in epoxy resin. Thin sections were stained with uranyl acetate and lead citrate, and observed with a Philips Tecnai 10 transmission electron microscope.

Statistics. Circular statistics were carried out with the Oriana program, using the Watson U^2 test to compare dispersion of orientations. Bead velocities in brain slices experiments were compared using Student's *t* test.

© 2010 Nature America, Inc. All rights reserved.

doi:10.1038/nn.2555